Available online at www.sciencedirect.com
ScienceDirect
Journal of Power Sources 166 (2007) 362–375
JOURNAL OF POWER SOURCES
www.elsevier.com/locate/jpowsour

Electrochemical reaction and performance of proton exchange membrane fuel cells with a novel cathode flow channel shape

Mu-Sheng Chiang [a,b], Hsin-Sen Chu [a,*], Cha'o-Kuang Chen [c], Sheng-Rui Jian [d]

[a] *Department of Mechanical Engineering, National Chiao Tung University, Hsin-Chu 30010, Taiwan*
[b] *Department of Mechanical Engineering, Nan Kai Institute of Technology, Nantou 54243, Taiwan*
[c] *Department of Mechanical Engineering, National Cheng Kung University, Tainan 70101, Taiwan*
[d] *Department of Electrophysics, National Chiao Tung University, Hsin-Chu 30010, Taiwan*

Received 13 December 2006; received in revised form 30 December 2006; accepted 2 January 2007
Available online 6 February 2007

Abstract

This study focuses on the investigation of the electrochemical reaction along a novel cathode flow channel of PEM fuel cells with various shoulder/channel (S/C) ratios at the outlet port. A three-dimensional mathematical model, considering conservation principles of mass, momentum, species and electric current is employed. Local variations of important model variables such as reactant concentration and local current density are presented by contour plots to elucidate the effects of channel geometry on transport process, catalyst reaction and cell performance. The potential fields of solid and membrane phases are also resolved in the cell domain and the driving force of the electrochemical reactions – the catalyst activation overpotential – is harnessed in modeling. Numerical calculations reveal the influence of the cathode channel configuration on the local distributions of various model variables. The results also show the dependence between optimal channel configuration and cell operating condition. At a medium reaction rate, the reaction sites underneath the shoulder region generate more current than the channel region. Therefore, a convergent channel configuration with a larger S/C ratio at the outlet port develops more current because such a design facilitates the electron transport and enhances local activation overpotential. However, as the cell voltage decreases and the reaction rate increases, such configuration loses its merit gradually as the requirement for a higher reactant concentration is more important and the reaction sites underneath the channel region have a higher reaction rate. Consequently, the divergent channel configuration with a lower S/C ratio of 0.67 performs better at a cell voltage of 0.22 V.

Keywords: Proton exchange membrane fuel cell; Shoulder/channel ratio; Electrochemical reaction; Activation overpotential; Cell performance

1. Introduction

Fuel cell technology has exhibited a potential in current energy technology due to the urgent requirement for renewable and environmentally friendly energy sources. Despite the long period of time since its first invention by Grove in 1839, it has received high interest during the past decades [1–3]. Enormous progress has been achieved on the topics of component design as well as on system integration [4–8]. The proton exchange membrane (PEM) fuel cell, with the merit of a quick start, high efficiency and a low operating temperature, is shown to be a promising candidate for future power sources in stationary and automotive applications. Its simple structure may be able to overcome the obstacles of the commercialization process such as the problems of cost and fuel supply.

The design of a flow delivery system plays an important role on cell performance. Methods include straight, serpentine and interdigitated flow channels and, according to their configuration, each design has specific merits. Recently, an interdigitated flow field has attracted attention due to the capability of expelling liquid water from the porous electrode, efficiently preventing a flooding problem and subsequent concentration overpotential. Through the utilization of two individual dead-end flow channels, the reactant is forced to flow through a diffusion layer by convection rather than by diffusion, and the shear force of the fluid is able to eject the liquid water in the pores. Other than the investigations of these three flow channel configurations, sophisticated modeling research on the PEM fuel cell are also seen in the literature [9–12]. Focusing on the influence of different flow field designs on the transport process and cell performance, West

* Corresponding author. Tel.: +886 3 571 2121x55115; fax: +886 3 5727930.
E-mail address: hschu@cc.nctu.edu.tw (H.-S. Chu).

0378-7753/$ – see front matter © 2007 Elsevier B.V. All rights reserved.
doi:10.1016/j.jpowsour.2007.01.084

Nomenclature

A	area (m^2)
c	molar concentration ($mol\ m^{-3}$)
C	form drag constant
D	diffusivity ($m^2\ s^{-1}$)
F	Faraday constant ($96{,}500\ C\ mol^{-1}$)
$\mathbf{g}$	gravitational acceleration ($m\ s^{-2}$)
i	current density ($A\ m^{-2}$)
j	transfer current density ($A\ m^{-3}$)
K	permeability (m^2)
L	length (m)
M	molecular weight ($kg\ mol^{-1}$)
n	number of species
$\mathbf{N}$	flux ($kg\ m^{-2}\ s^{-1}$)
P	pressure (Pa)
Q	volumetric flow rate ($m^3\ s^{-1}$)
r	rate constant
R	universal constant ($8.314\ J\ mol^{-1}\ K^{-1}$)
s	saturation level
S	source term
t	time
T	temperature (K)
$\mathbf{U}$	fluid velocity ($m\ s^{-1}$)
W	width (m)
x	molar fraction
y	mass fraction

Greek letters

α	switching function
β	transfer coefficient
ε	porosity
ϕ	potential (V)
η	overpotential (V)
φ	concentration dependence
μ	dynamic viscosity ($N\ s\ m^{-2}$)
ν	kinematic viscosity ($m^2\ s^{-1}$)
θ	contact angle
ρ	density ($kg\ m^{-3}$)
σ	electric conductivity ($S\ m^{-1}$)
τ	tortuosity
ς	surface tension ($N\ m^{-1}$)
ζ	stoichiometry of hydrogen or oxygen

Superscripts

c	capillary
e	effective value

Subscripts

a	anodic
act	activation
c	cathodic
cat	catalyst
cel	cell
con	condensation
eva	evaporation
ele	electrode
F	Forchheimer term
i	index for species
in	inlet port
j	index for species
m	membrane phase
ohm	ohmic
ref	reference
s	solid phase
sat	saturation
t	total
w	water

and Fuller [13] proposed a two-dimensional numerical analysis of the rib spacing in PEM electrode assemblies on current and water distribution within the cell. The results indicated that increasing the rib width strongly affected the membrane water content before the catalyst utilization is reduced. Therefore, the two-dimensional effect has a significant influence on water management. Kummer and Reddy [14] investigated the improvement of cell performance through optimization of channel dimensions and shape of the bipolar plates. In the recent study of Liu et al. [15–17], reactant gas transport and cell performance of PEMFCs with tapered flow field in channel depth as well as partially blocked flow channels were investigated through a two-dimensional model. Influence of liquid water formation on simulation result was included. The conclusions indicated that at the operating condition of high current density, the taper flow channels show remarkable beneficial effects in fuel transport, water management and cell performance. Also, the presence of baffles in the channel exhibited the same effects, especially at the locations beneath the baffles. Chiang and Chu [18] investigated the effects of transport components on the transport phenomena and performance of PEM fuel cells by using a three-dimensional model. The impacts of channel aspect ratio (AR) and GDL thickness were examined. It was found that a flat channel with a small AR or a thin GDL generates more current at low cell voltage due to the merits of better reactant gas transport and liquid water delivery.

These channels introduced a common feature that utilized a constant shoulder/channel (S/C) ratio along the main stream direction. It was shown in several studies [19–21] that the local electrochemical reaction of the PEM fuel cell as well as the current density exhibit high non-uniformity throughout the entire domain. In the study of Kulikovsky et al. [19], parametric study for the effect of transport properties such as carbon phase conductivity and oxygen diffusivity on local reaction rate was conducted by a two-dimensional half cell model. It was concluded that there exists a "dead zone" in the catalyst layer beneath the gas channel when the carbon phase conductivity is low. Consequently, the catalyst particles can be removed from this zone without significant performance loss. This method is also valid for higher values of conductivity with only trivial losses in current density despite the reaction being forced to proceed in the shoulder region of the catalyst layer. When

considering the effect of the reactant diffusion coefficient, the contribution of the catalyst layer under the flow channel on current generation is greater than that under the current collector if the oxygen diffusivity is poor. Therefore, the catalyst may be omitted in the region under the current collector. The improved two-dimensional agglomerate cathode model developed by Sun et al. [22,23] indicated that there exists a non-uniform cathode overpotential which is controlled by the channel-land geometry and operating condition, leading to an uneven electrode reaction rate. The results also revealed that increasing the channel-to-land width ratio leads to improved water transport and positively impacts the overall reaction rates at low cell voltage.

According to the previous discussions, it is clear that the transports of reaction gases as well as charged species exhibit a specific degree of influence on the cell performance according to the operating conditions and flow channel geometry. However, traditional design of flow field configurations with a fixed S/C ratio limits the flexibility of manipulating the local electrochemical reactions along the channel direction. The objective of this study is to explore a novel flow field design with continuous variation of S/C ratio along cathode channel by using a multi-physics model harnessing the major transport phenomena of PEM fuel cells. The factors of reaction gas transport and charged species conduction on cell local reaction rate are considered and discussed along the channel and transverse directions. To our knowledge, we report for the first time the numerical investigation of the effects of such novel cathode channel configurations.

2. Mathematical formulations

Fig. 1(a) illustrates the computational domain of current study. It consists of nine essential components of a single cell. A PEM is sandwiched by catalyst layers (CLs), gas diffusion layers (GDLs), flow channels and bipolar plates (BPs) on anode and cathode sides. As shown in Fig. 1(b), one feature of this paper is that through the assignment of two parameters W_s and W_c at cathode outlet port, the widths of channel and shoulder are varied continuously along the main stream direction.

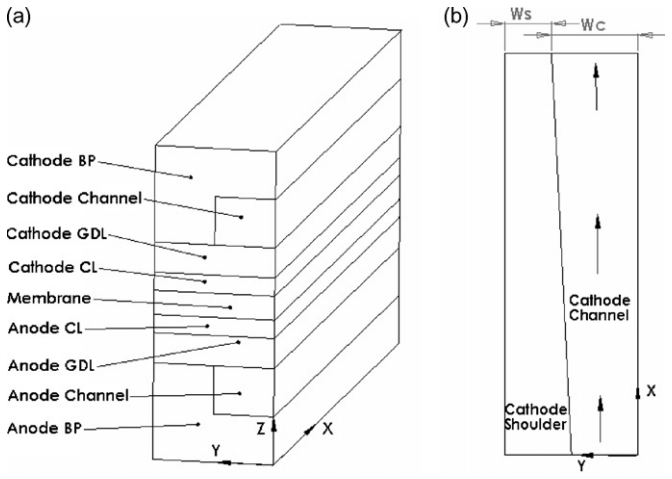

Fig. 1. (a) Computational domain and (b) cathode channel configuration.

There are many vital transport phenomena in the PEM fuel cells which are necessary to be considered during modeling. It is a multi-physics problem which requires several disciplines such as electrochemistry, electrics, material science, mass transport and fluid mechanics. Most importantly, the fuel cell undergoes a three-dimensional convection and diffusion process in the gas channels and other porous mediums. Also, the electrochemical reactions take place in catalyst layers of both electrodes. The reactant mass transport process is essentially multi-component mass transport and also concerns two-phase flow. Two charged particles, electrons and protons are driven by individual electric field. In the following, governing equations describing the major transport and electro-catalyst phenomena of PEM fuel cells are introduced. As the fluid flow and electric current transports are driven by different mechanism through separate routes, their model equations are presented in different section.

Basic assumptions are necessary in modeling development to simplify the mathematical analysis. The system is assumed to operate in steady and isothermal conditions. Due to low velocities and Reynolds numbers, the flows in anode and cathode are laminar. The materials of GDLs, CLs and PEM are modeled as porous media. The transport properties of fluids and electric conduction components are assumed constant and isotropic. Furthermore, the outer surfaces of BPs are regarded as constant electric potential.

2.1. Governing equations of fluid phase flow and mass transport

There are two main streams of gases supplied into the PEM fuel cell to achieve the energy releasing process, the anode and cathode gases. The former provides fuel for cell reaction and hydrogen is usually the main species. In addition, to facilitate the proton transport through membrane, suitable water vapor is necessary in the anode gas. The cathode feed gas participates the reduction reaction in cathode catalyst layer. Humidified pure oxygen or air is two of the candidates. The mechanism of these two bulk fluids transport throughout the cell domain is mainly by convection which is driven by the pressure gradient. Meanwhile, there is also mass diffusion for species in the reactant flows due to concentration gradient. The governing equations of this group are expressed as follows [18]:

- Mass conservation

$$\frac{\partial(\varepsilon^e\rho)}{\partial t} + \nabla\cdot(\varepsilon^e\rho\vec{U}) = 0 \tag{1}$$

- Momentum conservation

$$\frac{\partial(\varepsilon^e\rho\vec{U})}{\partial t} + \nabla\cdot(\varepsilon^e\rho\vec{U}\vec{U}) = -\varepsilon^e\nabla p + \nabla\cdot(\varepsilon^e\mu^e\nabla\vec{U}) + \varepsilon^e\rho_K\vec{g} - \frac{(\varepsilon^e)^2\mu^e\vec{U}}{K} + \frac{(\varepsilon^e)^3 C_F\rho\vec{U}|\vec{U}|}{K^{1/2}} \tag{2}$$

- Species conservation

$$\frac{\partial(\varepsilon^{\mathrm{e}}\rho y_i)}{\partial t} + \nabla\cdot(\varepsilon^{\mathrm{e}}\rho y_i \vec{U}\lambda_{\mathrm{g}}) = \nabla\cdot\left(\rho\sum_{j=1}^{n-1} D_{i,j}(\varepsilon^{\mathrm{e}})^{\tau}\nabla y_j\right) + S_i \tag{3}$$

- Liquid water transport

$$\nabla\cdot\left(\varepsilon^{\mathrm{e}}\rho\mathbf{U}k_{\mathrm{rl}}\frac{\nu}{\nu_{\mathrm{l}}}\right) + \nabla\cdot\mathbf{N}_{\mathrm{l}} = \nabla\cdot\left(\varepsilon^{\mathrm{e}}D^{\mathrm{c}}\nabla s - \frac{Kk_{\mathrm{rl}}k_{\mathrm{rg}}(\rho_{\mathrm{l}}-\rho_{\mathrm{g}})\mathbf{g}}{k_{\mathrm{rl}}\nu_{\mathrm{g}}+k_{\mathrm{rg}}\nu_{\mathrm{l}}}\right) + S_{\mathrm{l}} \tag{4}$$

In this study, all the cell components except bipolar plate and gas channel are modeled as porous medium with proper mass transport properties such as porosity and permeability. To unify the expression of model equation, a general type conservation equation is introduced throughout the interested domain including open channel and porous medium. Through simple dimensional analysis, in porous medium, the momentum equation can be reduced into Darcy equation which is usually employed in the study of such medium. The possibility of liquid water formation and transport is also included in this model. By way of comparing local vapor partial pressure and saturation pressure of water, information of water phase transition either condensation or evaporation is decided. Also, the main driving force of liquid water transport in electrodes and membrane is considered in Eq. (4).

The constitutive relations of mixture parameters and variables are listed as follows:

- Mixture density

$$\rho = \sum_{i=1}^{n}\rho_i(1-s) + \rho_{\mathrm{l}}s \tag{5}$$

- Effective porosity

$$\varepsilon^{\mathrm{e}} = \varepsilon(1-s) \tag{6}$$

- Saturation level

$$s = \frac{\rho_{\mathrm{g}}}{\rho_{\mathrm{l}}+\rho_{\mathrm{g}}} \tag{7}$$

- Effective viscosity

$$\mu^{\mathrm{e}} = \frac{\rho_{\mathrm{l}}s + \rho_{\mathrm{g}}(1-s)}{(k_{\mathrm{rl}}/\nu_{\mathrm{l}}) + (k_{\mathrm{rg}}/\nu_{\mathrm{g}})} \tag{8}$$

- Gas phase relative permeability

$$k_{\mathrm{rg}} = (1-s)^3 \tag{9}$$

- Liquid phase relative permeability

$$k_{\mathrm{rl}} = s^3 \tag{10}$$

- Binary diffusivity

$$D_{i,j} = \frac{0.0018583[T^{1.5}(M_i^{-1}+M_j^{-1})^{0.5}]}{P\psi_{ij}\Omega_{ij}} \tag{11}$$

- Capillary diffusion coefficient

$$D^{\mathrm{c}} = -\frac{Kk_{\mathrm{rl}}k_{\mathrm{rg}}[\varsigma\cos\theta_{\mathrm{c}}(\varepsilon^{\mathrm{eff}}/K)^{1/2} \times(-3.789s^2+3.338s-0.966)]}{k_{\mathrm{rl}}\nu_{\mathrm{g}}+k_{\mathrm{rg}}\nu_{\mathrm{l}}}. \tag{12}$$

2.2. Governing equations of electric currents

Due to oxidation and reduction reactions in the anode and cathode catalyst layers, two charged species, electrons and protons are generated on the anode side and consumed on the cathode side of the cell. Therefore, two separate electric fields build and dominate the transport of these two species. The solid phase of the catalyst layer and gas diffusion layer as well as the bipolar plate provide the passages for electron transport. Membrane phase of catalyst layer along with PEM takes charge of the ion transport. The general expression of current conservation in cell domain can be written as:

$$\nabla\cdot i_{\mathrm{s}} = -\nabla\cdot i_{\mathrm{m}} = -S_j \tag{13}$$

The solid and membrane phase current densities can be given from ohmic law:

$$i_{\mathrm{s}} = -\kappa_{\mathrm{s}}\nabla\phi_{\mathrm{s}} \tag{14}$$

$$i_{\mathrm{m}} = -\kappa_{\mathrm{m}}\nabla\phi_{\mathrm{m}} \tag{15}$$

The expression in Eq. (13) represents the local current density gradients or volumetric current densities, which are equal to zero except at the catalyst layers where electrochemical reactions take place. As a result, the solid phase current density decreases gradually toward membrane and the ionic phase current density increases toward the membrane direction in both CLs. The source term S_j connects these two phase currents transition, maintaining the current conservation property. Most importantly, it is the exact and ultimate mechanism that fulfills the energy transformation process in the PEM fuel cells. Vital ingredients that are necessary for such reaction include electrode properties, local reactant concentration and driving source-activation overpotentials in CLs. Its expression at anode and cathode sides can be expressed as below.

$$S_{\mathrm{a}} = A_{\mathrm{a}}j_{\mathrm{a,ref}}\left(\frac{c_{\mathrm{H_2}}}{c_{\mathrm{H_2,ref}}}\right)^{\varphi\mathrm{a}}\left[\exp\left(\frac{\beta_{\mathrm{a,a}}F\eta_{\mathrm{a,act}}}{RT}\right) - \frac{1}{\exp(\beta_{\mathrm{a,c}}F\eta_{\mathrm{a,act}}/RT)}\right] \tag{16}$$

$$S_{\mathrm{c}} = A_{\mathrm{c}}j_{\mathrm{c,ref}}\left(\frac{c_{\mathrm{O_2}}}{c_{\mathrm{O_2,ref}}}\right)^{\varphi\mathrm{c}}\left[\exp\left(\frac{\beta_{\mathrm{c,a}}F\eta_{\mathrm{c,act}}}{RT}\right) - \frac{1}{\exp(\beta_{\mathrm{c,c}}F\eta_{\mathrm{c,act}}/RT)}\right] \tag{17}$$

In regard to the model concerning the issue of current density and activation potential, there are two approaches in open literature. In early one-dimensional model [24], a current density was initially specified and the electrode overpotential as well as cell potential was solved subsequently through Tafel expression. A similar method was also employed in the study of Kazim et al. with a known value of electrode overpotential as input variable [25]. In this study, the methodology of Voltage-to-Current proposed by Nguyen et al. [26] is adopted. A unique feature of this algorithm is that it is able to provide local activation overpotential in catalyst layer. Its expression in Eqs (16)–(17) can be written as:

$$\eta_{\mathrm{act}} = \phi_{\mathrm{s}} - \phi_{\mathrm{m}} \tag{18}$$

In general, it has positive value in anode and negative value in cathode. The available cell potential is obtained from the knowledge of open cell voltage and a negative total cell overpotential that describes the entire potential loss between the two bipolar plates on anode and cathode. Expressions of these variables are expressed as:

$$\phi_{\mathrm{cel}} = 1.23 - 9 \times 10^{-4} \times (T - 298.15) + \frac{RT}{2F}\left(\ln P_{\mathrm{H_2}} + \frac{1}{2}\ln P_{\mathrm{O_2}}\right) + \eta_{\mathrm{t}} \tag{19}$$

$$\eta_{\mathrm{t}} = \eta_{\mathrm{ohm,a}} + \eta_{\mathrm{ohm,c}} + \eta_{\mathrm{act,a}} + \eta_{\mathrm{act,c}} + \eta_{\mathrm{m}}. \tag{20}$$

2.3. Connection between fluid phase flow and electric current

In the species conservation equation of Section 2.1, the source term S_i is introduced to consider the consumption or production of the species such as oxygen, hydrogen and water occurring in CLs. Hydrogen molecules are decomposed in anode catalyst layer as:

$$\mathrm{H_2} \rightarrow 2\mathrm{H^+} + 2\mathrm{e^-} \tag{21}$$

Meanwhile, oxygen molecules in cathode react with protons and electrons in cathode catalyst layer as:

$$\tfrac{1}{2}\mathrm{O_2} + 2\mathrm{H^+} + 2\mathrm{e^-} \rightarrow \mathrm{H_2O} \tag{22}$$

According to these two reactions, the source term for each species can be calculated and linked with Eqs. (16) and (17) as:

$$S_{\mathrm{H_2}} = 1.04 \times 10^{-8} S_{\mathrm{a}} \tag{23}$$

$$S_{\mathrm{O_2}} = 8.29 \times 10^{-8} S_{\mathrm{c}} \tag{24}$$

$$S_{\mathrm{H_2O}} = -9.33 \times 10^{-8} S_{\mathrm{c}} + S_{\mathrm{l}} \tag{25}$$

The term S_{l} in Eqs. (4) and (25) is used to consider the situation of water phase transition based on the following relation:

$$S_{\mathrm{l}} = M_{\mathrm{l}} r_{\mathrm{con}} \frac{\varepsilon^{\mathrm{e}} x_{\mathrm{w}}}{RT}(x_{\mathrm{w}} p - p_{\mathrm{sat}})\alpha + r_{\mathrm{eva}} \varepsilon^{\mathrm{e}} s \rho_{\mathrm{l}} (x_{\mathrm{w}} p - p_{\mathrm{sat}})(1-\alpha). \tag{26}$$

2.4. Boundary conditions and numerical procedure

According to Fig. 1, there are 9 components in this model with different transport and physical properties. An enormous mathematical system would be needed if these components are modeled and calculated separately. The unified domain formulation in previous sections prevents the tedious work on dealing with the boundary conditions between interfaces of various components. Only different transport and physical properties need to be set at different regions but using the same conservation equation and numerical algorithm.

For the boundary conditions of bulk flow equations, specific back pressures are assigned at outlet ports of channels. This is an important parameter for cell operating conditions. Another important factor of operating condition is channel inlet velocities which are based on the stoichiometric flow ratio as well as channel dimension. The volumetric flow rates at channel inlet ports are given as:

$$Q_{\mathrm{a}} = \frac{\zeta_{\mathrm{a}} i_{\mathrm{ref}} A_{\mathrm{ele}} R T_{\mathrm{a}}}{2F(P_{\mathrm{a}} - P_{\mathrm{sat,w,a}}) x_{\mathrm{H_2,in}}} \tag{27}$$

$$Q_{\mathrm{c}} = \frac{\zeta_{\mathrm{c}} i_{\mathrm{ref}} A_{\mathrm{ele}} R T_{\mathrm{c}}}{4F(P_{\mathrm{c}} - P_{\mathrm{sat,w,c}}) x_{\mathrm{O_2,in}}} \tag{28}$$

The saturation pressure of water in these two equations can be obtained from thermodynamic table or asymptotical relation which is a function of temperature.

For the solutions of potential fields in the calculation domain, specific solid phase potential levels are set on the outer boundaries of bipolar plates to gain the information of cell voltage as well as potential fields in cell domain. As the electrons are unable to penetrate the interface between CL and membrane due to the lacking of conduction medium, the solid phase potential gradient normal to this plane is zero. The same method is also used for membrane phase current at interface of CL and membrane. In addition to these conditions, there are symmetric and wall boundaries exist in the domain. The normal gradients of model variables, concentration or potential are set as zero to ensure the symmetrization or impermeability of the transport quantities such as mass flux or current density. Furthermore, non-slip condition is used for velocity field on the interface between channel and BP.

The model equations introduced are coupled and nonlinear. Therefore, the variables appearing in model equations must be solved by employing numerical method. The continuous cell domain is discretized into several control volumes with dependent variables calculated and stored in center of each computational cell to ensure the conservation properties of physical quantities. A general purpose CFD software with the SIMPLE algorithm based solver [15,27–29] is utilized in the solution processes. The velocity fields in momentum equation are solved at first with a pressure correction process followed to consider the mass imbalance. After the velocity and pressure fields are corrected, the concentration equation and potential equations are solved subsequently.

Rigorous numerical tests have been performed to ensure the independence between the solution and the grid size. A grid

Table 1
Main cell parameters, properties and operating conditions

Gas channel length, 6.0E−2 m	Diffusion layer porosity, 0.4
Gas channel thickness, 1.0E−3 m	Catalyst layer porosity, 0.28
Diffusion layer thickness, 2.54E−4 m	Membrane porosity, 0.28
Catalyst layer thickness, 1.0E−5 m	Diffusion and catalyst layer permeability, 2.3E−11 m^2
Membrane thickness, 1.75E−4 m	Membrane permeability, 1.0E−18 m^2
Gas channel half width (inlet port), 5.0E−4 m	Reactant relative humidity, 100%
Shoulder width (inlet port), 5.0E−4 m	Oxygen mass fraction at channel inlet port, 0.196
Cathode inlet velocity, 0.84 m s^{-1}	Vapor mass fraction at cathode inlet port, 0.160
Anode inlet velocity, 0.35 m s^{-1}	Vapor mass fraction at anode inlet port, 0.733
Cell back pressure, 2 atm	Hydrogen mass fraction at anode inlet port, 0.267
Cell temperature, 80 °C	Electrode conductivity, 114 S m^{-1}

system with about 86,400 cells is found to provide satisfactory results. The dependent variables are calculated during each iteration cycle and the convergence criterion is imposed that the relative residual for each variable between two adjacent iterations is smaller than 1.0E−4. Details of the numerical procedure as well as model validation process can be found in previous works [18,30].

3. Results and discussion

In a PEM fuel cell, the components for reactant and current transport play an important role and impose great influence on cell performance. To study the effects of novel flow field configuration design, the width of the cathode channel outlet port is varied by using five S/C ratios with a constant value of 1 at the inlet port. Table 1 lists the main cell parameters, properties and operating conditions used in this study. The corresponding reactant stoichiometry for anode and cathode inlet velocities in base case is 3. Employed data for various simulation cases are shown in Table 2. According to the S/C ratio parameter, the channel configuration can be cataloged into divergent (case A and B), straight (case C) and convergent (case E and F) channels.

3.1. Reactant species transport and concentration distribution

The main purpose of the flow field in fuel cell is to deliver reactant throughout the cell domain. Furthermore, product from electrochemical reaction and non-reaction gas such as water and nitrogen should be carried out of the cell to provide space for fresh gas transport. Fig. 2 shows the oxygen mass fraction contour on middle horizontal plane of cathode catalyst layer at cell voltage of 0.62 and 0.22 V for cathode channel configurations with S/C ratio of 0.67, 1 and 1.5. Note that the straight line drawn in the contour represents the boundary between channel and shoulder which indicates clearly what category the channel design is belong to. Vertical boundary lines in each contour represent the central region of shoulder (left) and channel (right) due to the adoption of the symmetric model domain. It is shown from Fig. 2 that the oxygen concentration distributions depend on cell operating conditions, positions as well as channel geometries. Clearly, the higher oxygen concentration locates close to the inlet port of channel and decreases gradually toward the channel downstream and shoulder region because the cell reaction consumes oxygen. Also, this explains the reason that the oxygen concentration is larger at cell voltage of 0.62 V as the reaction is not so fast than that at 0.22 V. Furthermore, these plots disclose the effect of channel geometry on the reactant transport for various operating conditions. At cell voltage of 0.62 V, the divergent channel (case A) provides more even and higher reactant concentration than other designs due to its greater exposed area of catalyst layer under channel region. The same phenomenon is also found at 0.22 V condition. From Fig. 2, the lowest oxygen concentration locates at shoulder region of channel down stream. Since the transverse transport of reactant is mainly due to diffusion, a larger S/C ratio at channel outlet port such as case E corresponds to a larger diffusion length, such that the oxygen is difficult to reach the shoulder central (left boundary of contour) region of the catalyst layer.

Another important factor that influences the reactant transport in cathode is the liquid water saturation level. In Fig. 3, contours of liquid water saturation are shown at the same condition and location of Fig. 2. The influence of channel geometry on this factor is clearly seen. In general, the shoulder region of catalyst layer accumulates more liquid than channel region because the latter is close to the main stream of channel. The liquid water formed from cell reaction at this region is easy to transport out of the cell. However, at shoulder central of convergent channel

Table 2
Simulation cases for various channel configurations used in this study

	A[a] Divergent channel[b]	B[a] Divergent channel[b]	C[a] Straight channel[b]	D[a] Convergent channel[b]	E[a] Convergent channel[b]
W_s (S)	0.4 mm	0.45 mm	0.5 mm	0.55 mm	0.6 mm
W_c (C)	0.6 mm	0.55 mm	0.5 mm	0.45 mm	0.4 mm
S/C ratio (W_s/W_c)	0.67	0.82	1.00	1.22	1.5

[a] Case.
[b] Description.

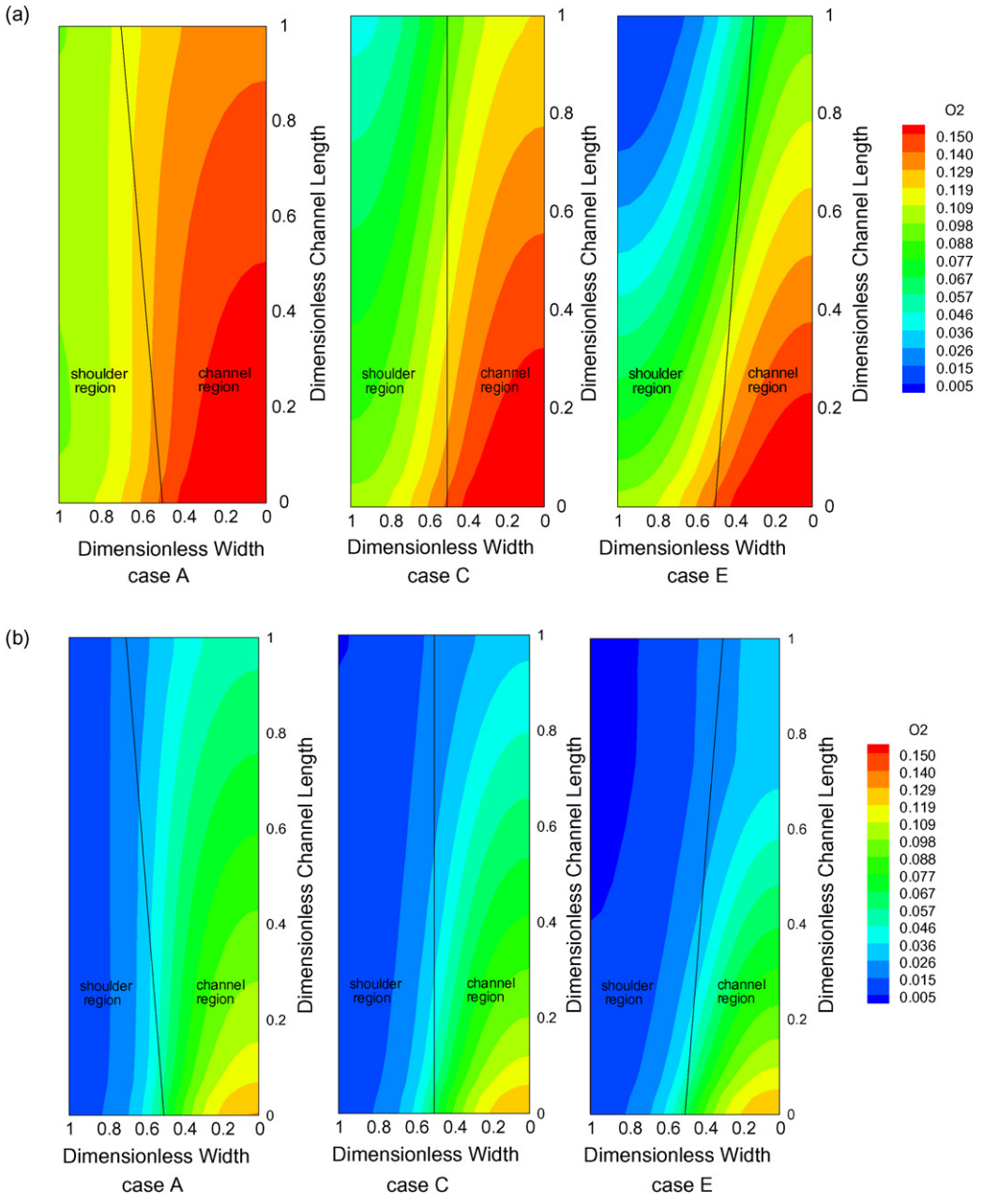

Fig. 2. Oxygen mass fraction contours at cell voltage of (a) 0.62 V and (b) 0.22 V for outlet port S/C values of 0.67, 1 and 1.5.

(case E) downstream, large amount of liquid water is accumulated due to its long transport path, especially at low cell voltage of 0.22 V. Because the pore space available for reactant diffusion is clogged by liquid water, it manifests the result of relative lower oxygen concentration shown in Fig. 2.

3.2. *Potential fields and activation overpotential distribution*

Not only the mass transport variables are influenced by the design of channel geometry, the potential field distributions and electric currents are also affected. In fuel cell modeling investigation, the term overpotential is frequently mentioned in the literature. In general, it stands for the potential variation or loss in the cell region. As the electric conductivities of solid and membrane phase materials are finite, the electric resistances cause a certain degree of potential drop in two different positions when currents flow through them. Meanwhile, at a fix point in the CL, there exist two phase potentials and a local potential gap is built between solid and membrane phase materials. Such a potential gap represents another form of loss or irreversibility in a fuel cell. However, more importantly, it drives the process of electrochemical reaction.

Fig. 4 presents the distribution of the two phase potential fields on middle plane of cathode catalyst layer for the model with straight channel geometry. Note that in this study, a value of total cell overpotential is designated on the outer surface of cathode bipolar plate while that of anode bipolar plate is assigned

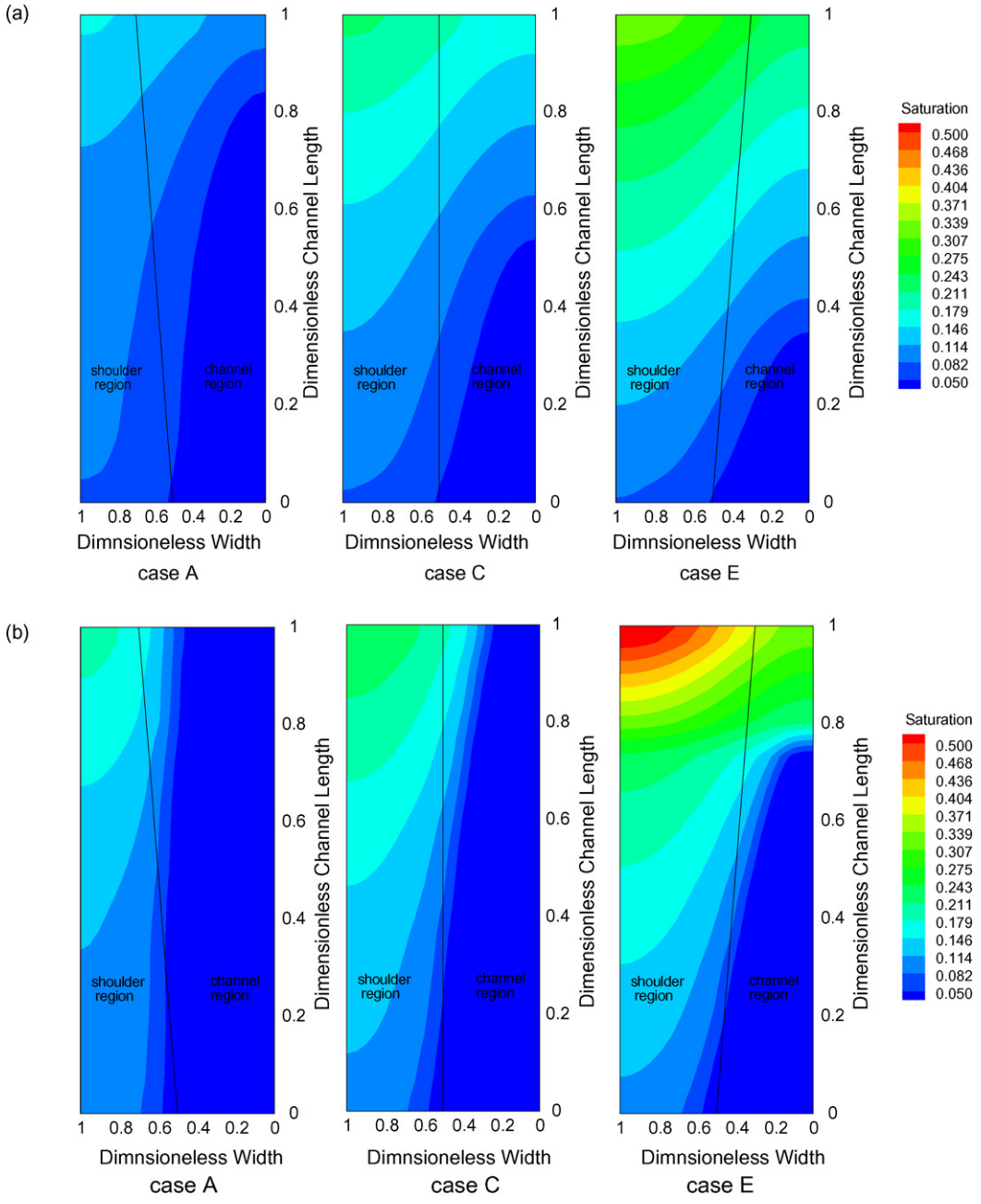

Fig. 3. Liquid water saturation contours at cell voltage of (a) 0.62 V and (b) 0.22 V for outlet port S/C values of 0.67, 1 and 1.5.

as the reference potential level. From the fact that the negative charged species moves from lower potential to higher potential, also the positive charged species moves in the opposite direction, this figure discloses some interesting points which are worth further discussion. It is shown from the contour plots that the solid phase potential increases from shoulder region to channel region, meaning that the electrons at the cathode mainly move in this direction to participate the electrochemical reaction in CL. At cell voltage of 0.62 V, the potential distribution has a more uniform distribution along channel direction than that at 0.22 V, indicating that at this operating condition, local cell reaction and current flow are uniform. Nevertheless, at cell voltage of 0.22 V, the reaction sites at upper stream shoulder region exhibit greater potential deviation from the designated cathode boundary potential, meaning that there are stronger cell reaction and solid phase current density than downstream shoulder region of catalyst layer. Also showed in Fig. 4, the membrane phase potential contours reveal a different variation trend. At cell voltage of 0.62 V, upper stream catalyst layer beneath shoulder exhibits a stronger potential drop than that beneath channel. However, this position shifts to the channel region at cell voltage of 0.22 V. This may reflect a fact that such a great membrane phase potential drop could be attributed to a stronger electrochemical reaction at this location or smaller membrane conductivity due to low water content.

With the information of these two potential fields, the activation overpotential in CL can readily be obtained. Fig. 5 depicts the contours of this variable for three different channel designs at

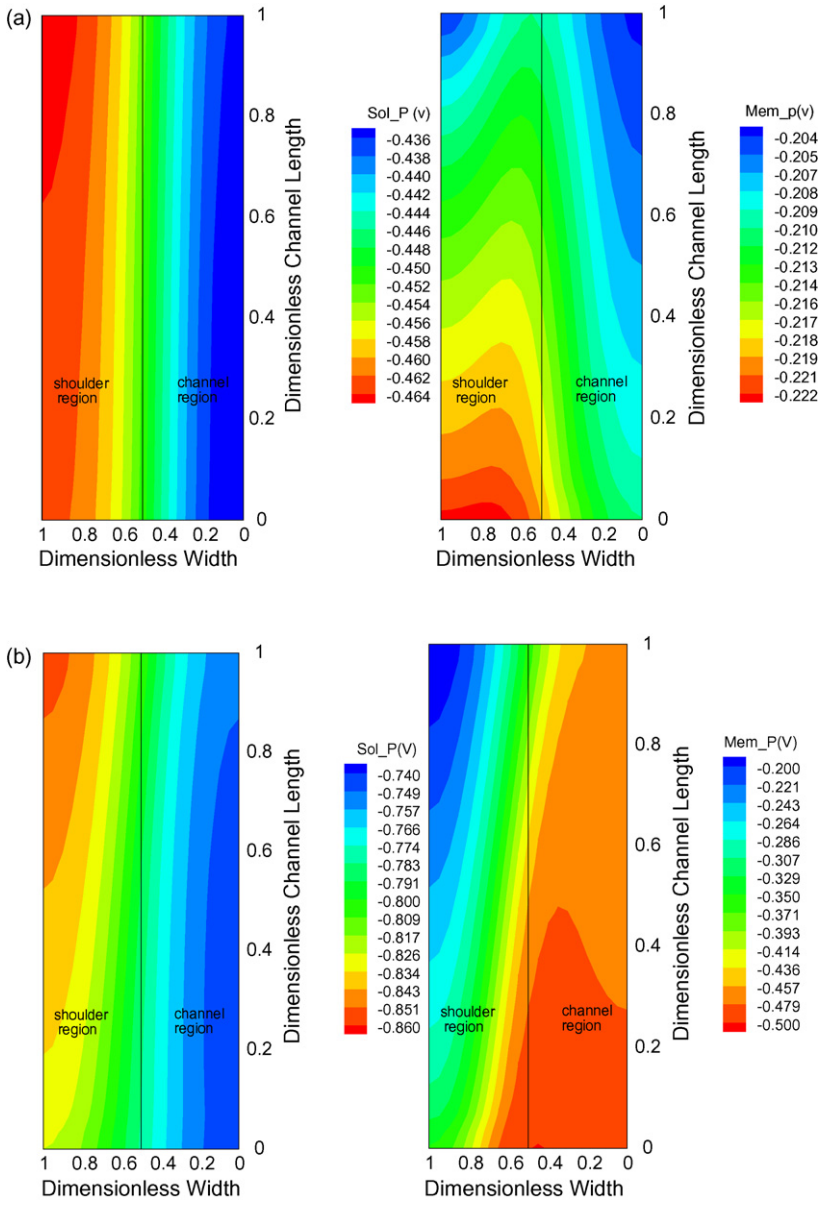

Fig. 4. Solid and membrane phase potential contours at cell voltage of (a) 0.62 V and (b) 0.22 V for straight channel.

cell voltages of 0.62 V and 0.22 V. It is noted that in Eq. (17) the term of cathode activation overpotential appears in two exponential expressions. Therefore, the negative sign can be neglected when judging its strength of electrochemical driving force. It is found from this figure that in general, catalyst layer underneath shoulder region exhibits greater activation overpotential than that below channel region no matter what the cell voltage is. This is essentially due to smaller solid phase potential variation at shoulder region because the electrons migrate from shoulder to channel. Also, at channel down stream this value is larger than that at up stream. Considering the effect of channel geometry on this variable, it is found that a fuel cell with divergent channel produces more uniform distributions; meanwhile, a convergent channel design fuel cell generates higher activation overpotential at shoulder region of channel down stream. However, this additional driving force may not be able to generate corresponding higher current along because the oxygen concentration at this region should be taken into account.

3.3. Local catalyst reaction rate

Base on Eqs. (16)–(17), the catalyst reactions in a fuel cell require two important factors – the reactant concentration and activation overpotential. According to the discussion in previous sections, it is evident that distributions of these two properties exhibit entirely different variation trends according to the operating condition and position. Therefore, the local cell reaction rate is expected to be non-uniform and requires further investigation.

Fig. 6 illustrates the current density contours for the same channel configurations and operating conditions as previous figures. A manifest transition where higher local reaction takes place between medium and high reaction rates is clearly seen,

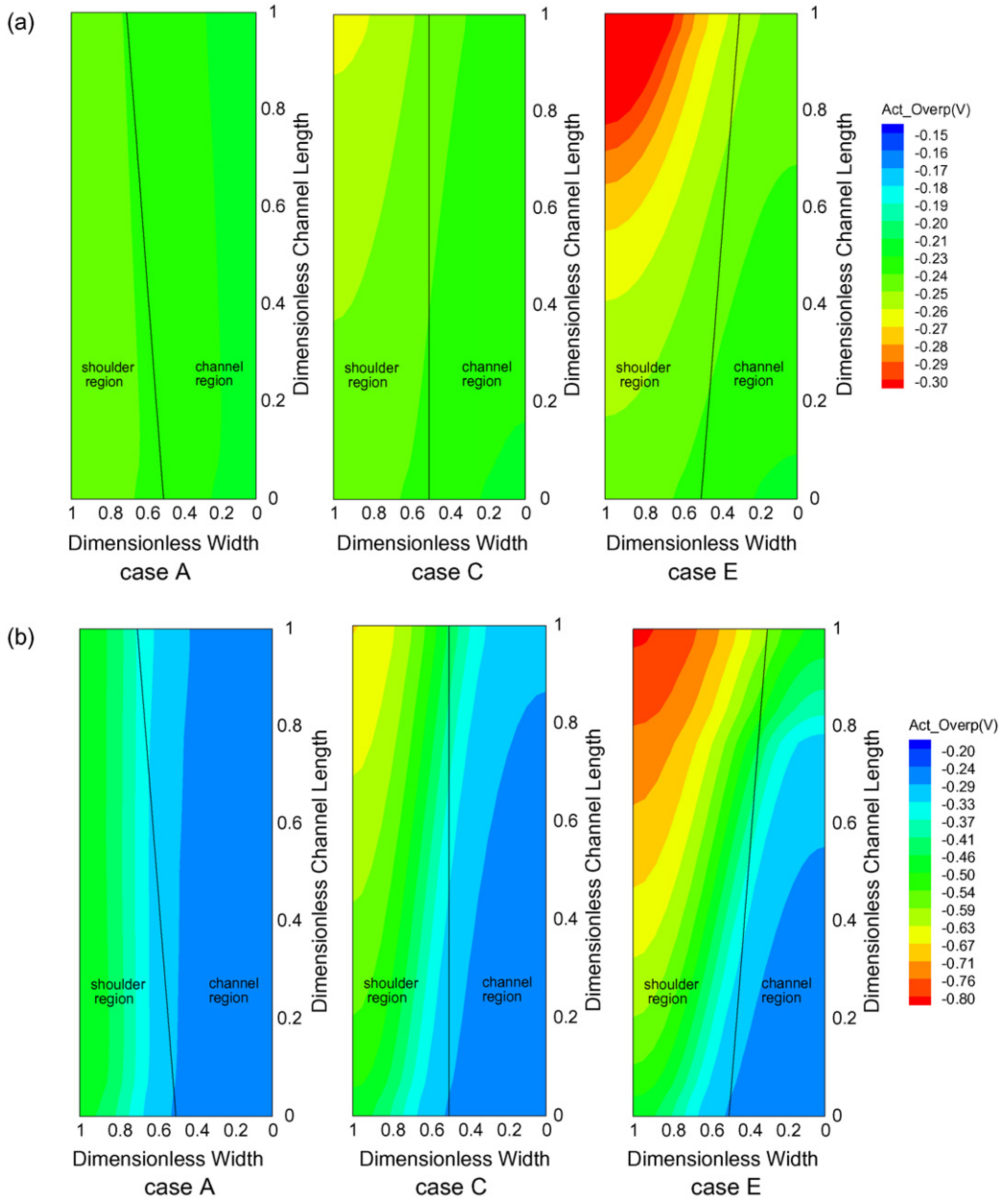

Fig. 5. Activation overpotential contours at cell voltage of (a) 0.62 V and (b) 0.22 V for outlet port S/C values of 0.67, 1 and 1.5.

no matter what channel geometry is. At cell voltage of 0.62 V, the plot indicates that most current generated around shoulder region of catalyst layer. However, the higher reaction rate zone moves toward the interface between shoulder and channel regions as the cell voltage decreases to 0.22 V. This is because that when cell operates at 0.62 V, the electrochemical reaction is not so strong, therefore the high concentration reactant does not contribute completely to the cell reaction. On the contrary, the activation overpotential plays a more important role on the local current generation, making the position of higher cell reaction locates at shoulder central of channel upper stream. At 0.22 V operating voltage, the catalyst reaction is increased and high concentration reactant is needed for the reaction. This fact causes the high current density position moves toward the channel direction where perfect combination of concentration and activation exists. Therefore, despite the fact that channel central region has greater oxygen concentration than other place, it dose not generate corresponding high current because the activation overpotential is the lowest.

According to these discussions, the effects of channel outlet port S/C ratio for different operating conditions can also be found in Fig. 6. At high cell voltage, a larger S/C ratio design creates more region of high current density such as case E of Fig. 6(a). However, this design leads to a low current density zone around downstream shoulder central at 0.22 V and a smaller S/C ratio design such as case A is found to have better performance.

In order to elucidate the local dominate mechanism of cell reaction, Fig. 7 depicts the transverse distributions of local oxy-

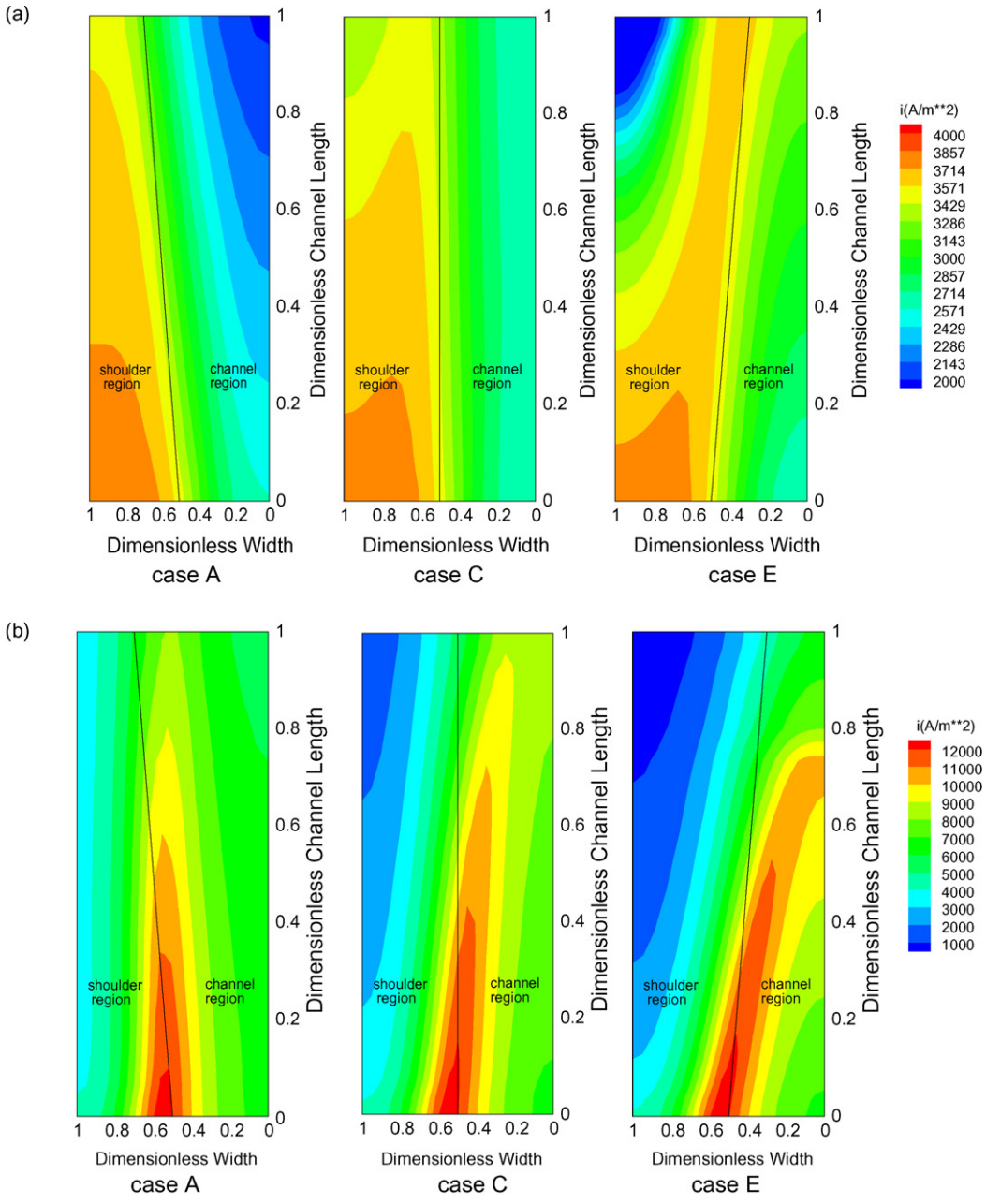

Fig. 6. Current density contours at cell voltage of (a) 0.62 V and (b) 0.22 V for outlet port S/C values of 0.67, 1 and 1.5.

gen mass fraction and local current density at 0.62 V cell voltage and S/C values of 0.67, 1.50. The position is on the same plane of previous figures at $x = 0.012$ m and 0.048 m. It is found from Fig. 7(a) that around channel upper stream, although a divergent channel such as S/C equal to 0.67 provides higher reactant concentration, its reaction rate is smaller than the convergent channel design, meaning that at this operating condition, conduction overpotential dominates local cell reaction. That is, a channel design with wider shoulder offers a less resistance passage for the transverse transport of electrons and the potential loss is smaller than that with narrower shoulder. Therefore, the convergent channel design has larger activation overpotential and higher local reaction rate. The plot in Fig. 7(b) exhibits a stronger variation of current density and oxygen concentration between divergent and convergent channel designs. Due to a wider shoulder, the design with 1.50 S/C value at outlet port results in a relatively lower level of oxygen concentration, especially at shoulder region. Consequently, the shoulder region of convergent channel is dominated by the concentration overpotential and the channel region is dominated by the conduction overpotential. On the contrary, because of the higher oxygen concentration level provided by the divergent channel, the transverse local current density exhibits the conduction overpotential dominated mechanism for cell reaction.

Comparison of local current density between convergent and divergent channel designs at high cell reaction rate is shown at Fig. 8(a and b). At position of $x = 0.012$, the oxygen concentration distributions has a similar variation trend with that at

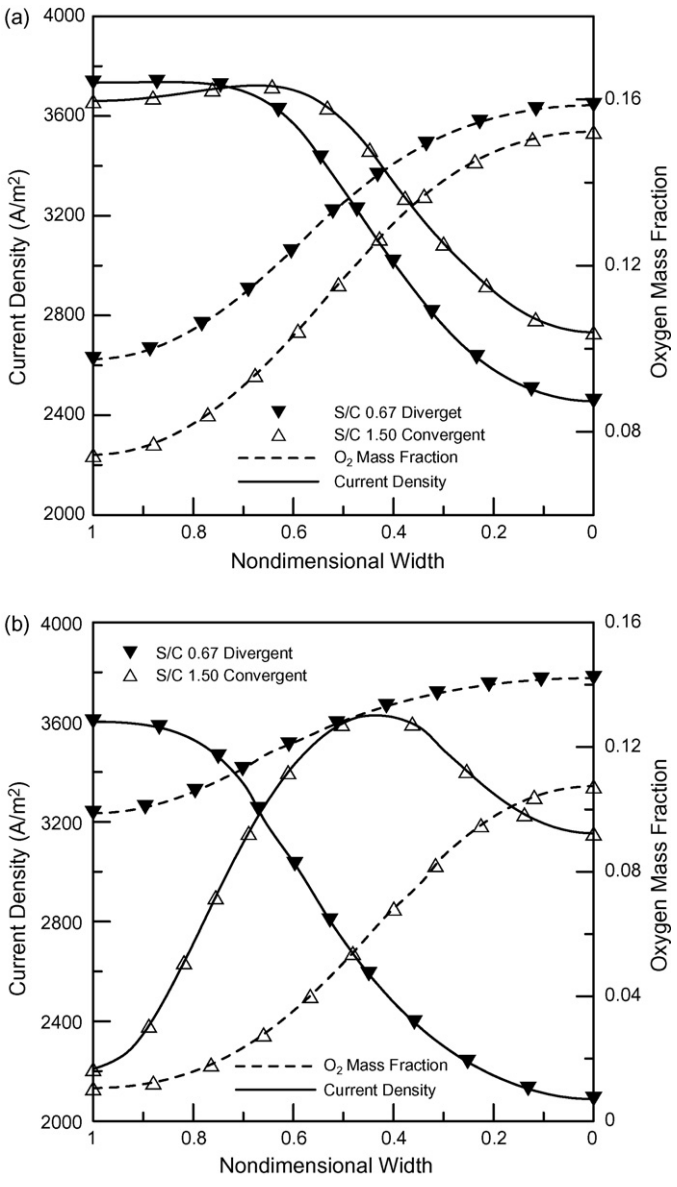

Fig. 7. (a) Transverse oxygen mass fraction and current density at $x = 0.012$ m of CL middle plane with cell voltage of 0.62 V and S/C values of 0.67, 1.50. (b) Transverse oxygen mass fraction and current density at $x = 0.048$ m of CL middle plane with cell voltage of 0.62 V and S/C values of 0.67, 1.50.

0.62 V. Also, the channel regions of these two channel configuration still exhibit conduction dominate mechanism at 0.22 V cell voltage. Nevertheless, a clear transition exists at domain central that change the relative magnitude of current densities at shoulder region for these two channel designs. This is attributed to the extremely low level of oxygen concentrations around shoulder regions at 0.22 V cell voltage. However, at downstream region the convergent channel design is entirely dominated by concentration overpotential and the variation trends between local current density and oxygen concentration are consistent in Fig. 8(b). This reflects a fact that a convergent channel configuration is unable to offer sufficient reactant concentration at channel downstream region when the cell reaction rate is high.

3.4. Cell performance for channel design with various S/C ratios

In order to provide a quantitative comparison of the novel flow channel design, the bar chart of average current density at various cell voltages is shown in Fig. 9 for five cathode outlet port S/C ratios. This figure indicates the transition of better cell channel design with operating voltage. At cell voltage of 0.22 V, divergent channel with S/C ratio of 0.67 creates the greatest current density than other cases. This is because that at such a high reaction rate, more oxygen can be transported to the reaction sites under the channel region for this channel configuration. However, as the average reaction slows down and cell voltage increases, this characteristic gradually lost its importance. Con-

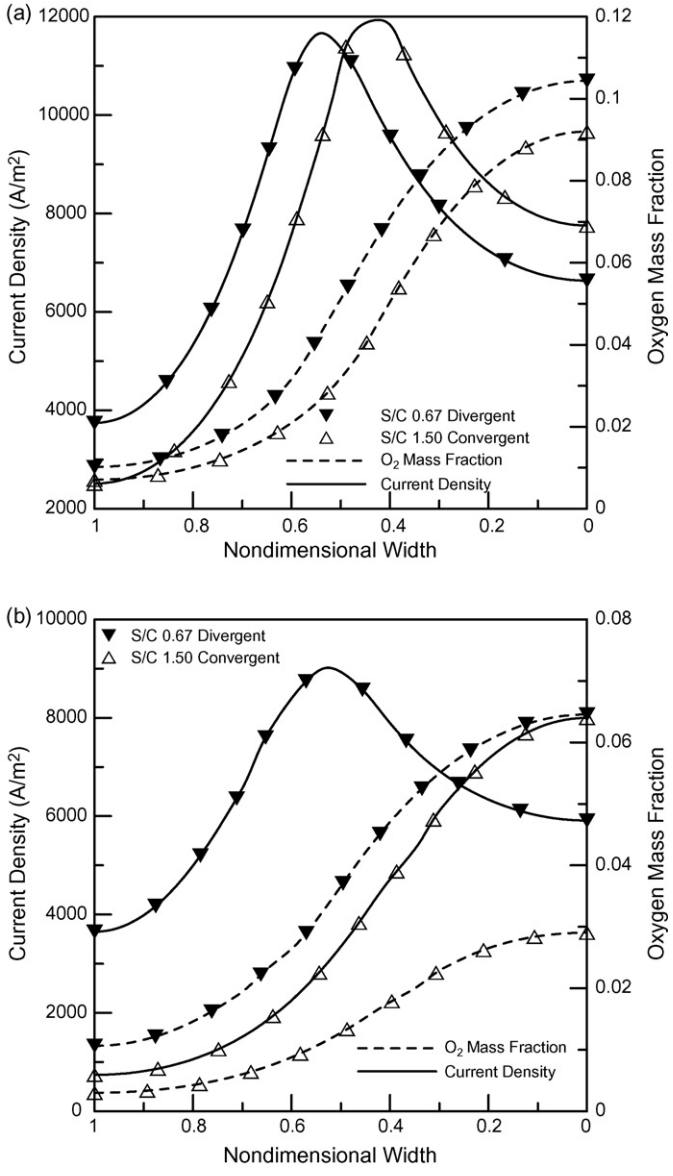

Fig. 8. (a) Transverse oxygen mass fraction and current density at $x = 0.012$ m of CL middle plane with cell voltage of 0.22 V and S/C values of 0.67, 1.50. (b) Transverse oxygen mass fraction and current density at $x = 0.048$ m of CL middle plane with cell voltage of 0.22 V and S/C values of 0.67, 1.50.

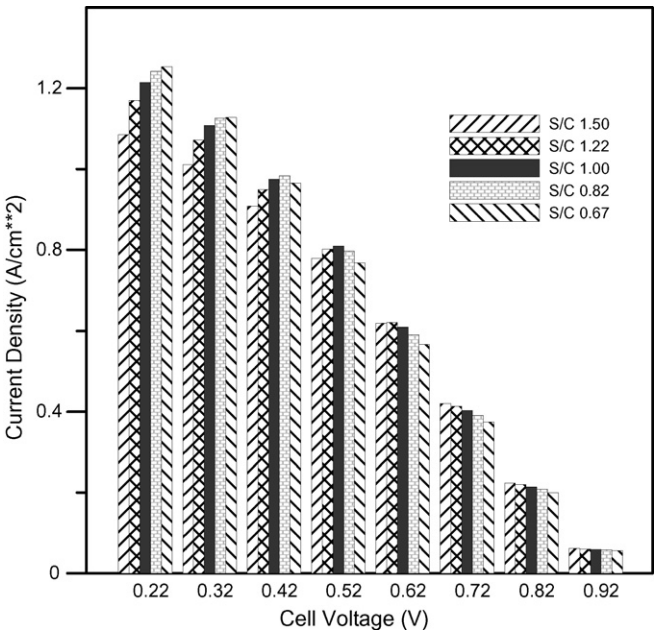

Fig. 9. Comparison of cell performance for various cathode channel geometry designs.

trarily, a smaller S/C design which offers wider shoulder region becomes more beneficial for the cell reaction because it facilities the electrons transport to the catalyst layer and enhances the activation overpotential.

3.5. Effect of reactant stoichiometry on cell performance

As the reactant flow rates have significant impact on cell performance, it is instructive to examine the effect of reactant stoichiometry on reaction rate. Fig. 10 shows the cell output current densities for three values of reactant stoichiometry at cell voltages of 0.22 and 0.62 V. It is found that the influence of reactant stoichiometry is obvious at lower cell voltage such as 0.22 V. When the reactant stoichiometry is low, less fuel and oxygen are supplied into the cell so the corresponding output current density is small. In such circumstance, the role of channel geometry on cell performance is vital. Fig. 10 reveals that when the stoichiometry is 2, larger variations of output current exist among the three different channel shapes. This is attributed to the fact that at 0.22 V, more reactants are required to fulfill electrochemical reactions. Therefore, the reductions of stoichiometry and reactant flow rate enhance the important role of channel geometry design. However, such tendency decreases as the stoichiometry increases to 4 because the fertile reactant flow rate makes the role of channel geometry less important than that at stoichiometry of 2.

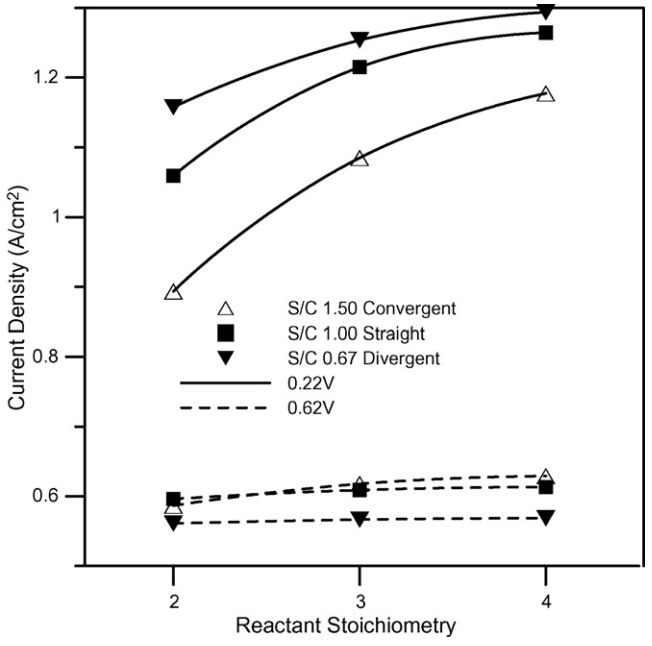

Fig. 10. Effect of reactant stoichiometry on cell current density at operating voltages of 0.22 and 0.62 V for three cathode channel configurations.

At a medium cell voltage, the reactant stoichiometry effect on current density is minor as the electrochemical reaction is dominated by conduction and activation overpotentials. However, a close inspection of Fig. 10 indicates that it presents a relatively larger influence on current density for the convergent shape channel. Despite the greater shoulder region of such channel configuration facilitates electrons transport to reaction sites and enhances output current, the cell reaction rate is reduced at lower stoichiometry as the reactant concentration is relatively small. This phenomenon reflects the need of detail inspection of the impact for various operating parameters on such novel flow channel. A systematic study on this issue is currently undergoing by our group.

4. Conclusion remarks

An investigation of the effects of a novel flow channel with various outlet port S/C ratios in a PEM fuel cell on the transport phenomena and catalyst reaction has been performed through a three-dimensional multi-component model. The influence of the channel geometry on local oxygen, potential and current density distributions are examined in detail. According to the results and discussion, the following conclusions can be drawn:

1. The configuration of flow channel influences the distribution of various transport variables such as reactant concentration, saturation level, potential field and activation overpotential.
2. For a narrower channel with large S/C ratio at outlet port, the average passage for electron conduction to the reaction site is shorter, such that it can generate more current at medium cell voltage where the activation overpotential dominates the catalyst reaction.
3. With the increase of cell reaction rate, the requirement for high reactant concentration becomes more important. Therefore, the best channel geometry shifts toward the design with a small S/C outlet port ratio, which offers a shorter transport passage for oxygen around channel region.
4. The saturation level of liquid water also has an important effect on oxygen transport and cell reaction rate, especially at low cell voltage. Consequently, the divergent channel design creates higher current density at such operating condition as

the liquid water is easy to transport out of the channel from the outlet port.

5. Transverse plots of local current density and oxygen concentration demonstrate the dominant mechanism of local cell reaction. When the variation trends between these two parameters are consistent, the cell reaction is dominated by concentration overpotential. Otherwise, it is controlled by conduction and activation overpotentials.
6. The reactant stoichiometry effect on the cell performance is quite obvious at lower cell voltages where a great amount of fuel and oxygen are required to fulfill the electrochemical reactions. Furthermore, it has a greater influence on the output current among different channel geometries at a value of 2.

References

[1] P. Costama, S.S. Srinivasan, J. Power Sources 102 (2001) 242–252.
[2] P. Costama, S.S. Srinivasan, J. Power Sources 102 (2001) 253–269.
[3] M.L. Perry, T.F. Fuller, J. Electrochem. Soc. 149 (2002) S59–S67.
[4] D. Song, Q. Wang, Z. Liu, T. Navessin, M. Eikerling, S. Holdcroft, J. Power Sources 126 (2004) 104–111.
[5] S.R. D'Souza, J. Ma, C. Wang, J. Electrochem. Soc. 153 (2006) A1795–A1799.
[6] A.F. Gullá, M.S. Saha, R.J. Allen, S. Mukerjee, J. Electrochem. Soc. 153 (2006) A366–A371.
[7] S. Gamburzev, A.J. Appleby, J. Power Sources 107 (2002) 5–12.
[8] V. Mehta, J.S. Cooper, J. Power Sources 114 (2003) 32–53.
[9] K. Haraldsson, Keith Wipke, J. Power Sources 126 (2004) 88–97.
[10] R. Sousa Jr., E.R. Gonzalez, J. Power Sources 147 (2005) 32–45.
[11] D. Cheddie, N. Munroe, J. Power Sources 147 (2005) 72–84.
[12] A.Z. Weber, J. Newman, Chem. Rev. 104 (2004) 4679–4726.
[13] A.C. West, T.F. Fuller, J. Appl. Electrochem. 26 (1996) 557–565.
[14] A. Kummer, R.G. Reddy, J. Power Sources 113 (2003) 11–18.
[15] H.C. Liu, W.M. Yan, C.Y. Soong, F. Chen, J. Power Sources 142 (2005) 125–133.
[16] C.Y. Soong, Y.M. Yan, C.Y. Tseng, H.C. Liu, F. Chen, H.S. Chu, J. Power Sources 143 (2005) 36–47.
[17] H.C. Liu, W.M. Yan, C.Y. Soong, F. Chen, H.S. Chu, J. Power Sources 158 (2006) 78–87.
[18] M.S. Chiang, H.S. Chu, J. Power Sources 160 (2006) 340–352.
[19] A.A. Kulikovsky, J. Divisek, A.A. Kornyshev, J. Electrochem. Soc. 146 (1999) 3981–3991.
[20] H. Meng, C.Y. Wang, J. Electrochem. Soc. 151 (2004) A358–A367.
[21] B.R. Sivertsen, N. Djilali, J. Power Sources 141 (2005) 65–78.
[22] W. Sun, B.A. Peppley, K. Karan, Electrochim. Acta 50 (2005) 3359–3374.
[23] W. Sun, B.A. Peppley, K. Karan, J. Power Sources 144 (2005) 42–53.
[24] T.E. Springer, T.A. Zawodzinski, S. Gottesfeld, J. Electrochem. Soc. 138 (1991) 2334–2342.
[25] A. Kazim, H.T. Liu, P. Forges, J. Appl. Electrochem. 29 (1999) 1409–1416.
[26] P.T. Nguyen, T. Berning, N. Djilali, J. Power Sources 130 (2004) 149–157.
[27] S.V. Patankar, Numerical Heat Transfer and Fluid Flow, Hemisphere, New York, 1980.
[28] J.J. Hwang, C.K. Chen, R.F. Savinell, C.C. Liu, J. Wainright, J. Appl. Electrochem. 34 (2004) 217–224.
[29] CFD-ACE(U)^{TM} User Manual, CFD Research Corp., Huntsville, AL 20054.
[30] M.S. Chiang, H.S. Chu, Proc. IMechE Part A, J. Power Energy 220 (2006) 42–53.